CrystEngComm

www.rsc.org/crystengcomm

Volume 15 | Number 13 | 7 April 2013 | Pages 2339–2550

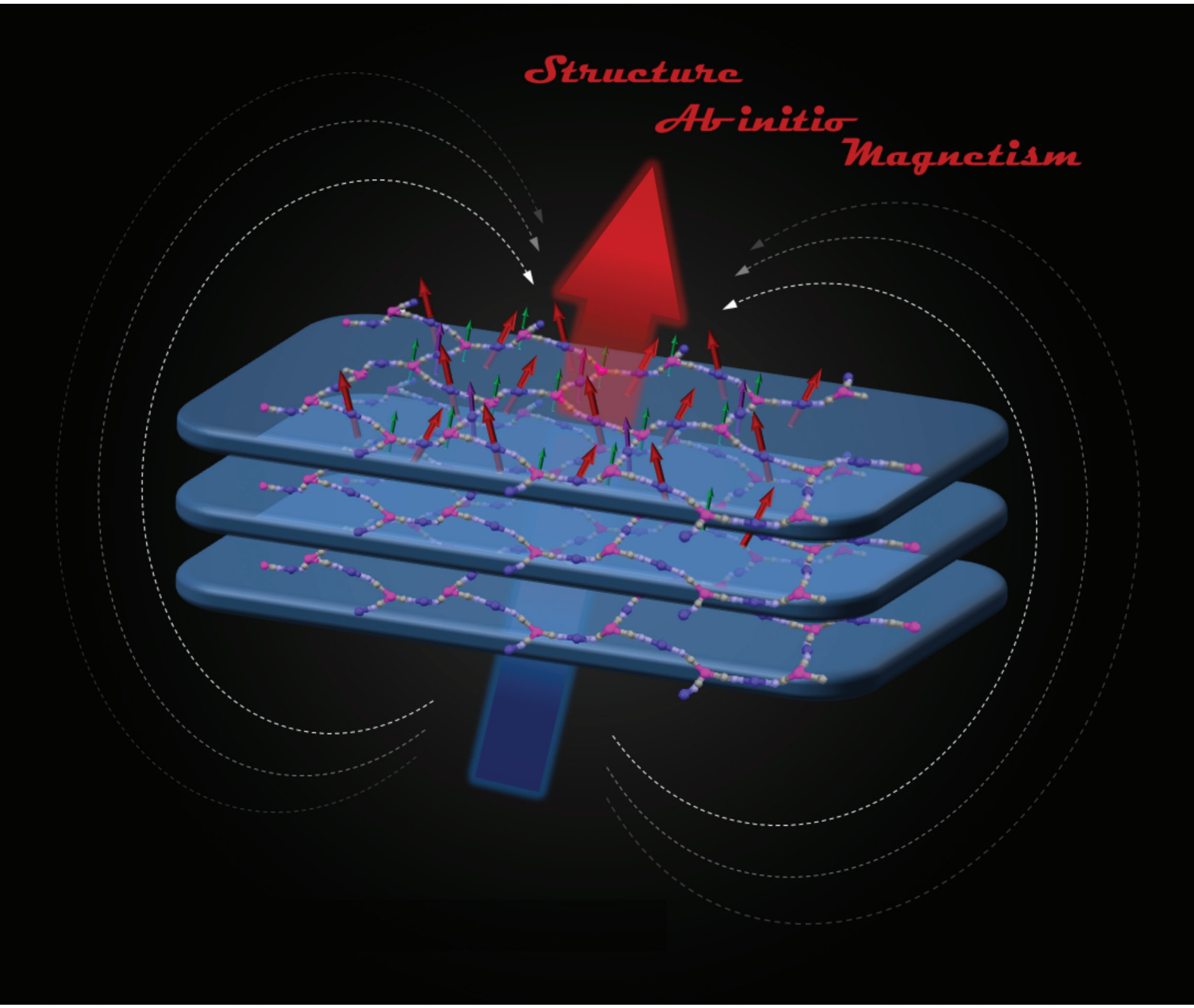

RSC Publishing

COVER ARTICLE

Podgajny *et al.*

Magnetic anisotropy of Co^{II}–W^{V} ferromagnet: single crystal and *ab initio* study

CrystEngComm

RSC Publishing

PAPER

View Article Online
View Journal | View Issue

Cite this: *CrystEngComm*, 2013, **15**, 2378

Magnetic anisotropy of Co^{II}–W^{V} ferromagnet: single crystal and *ab initio* study†

Szymon Chorazy,[a] Robert Podgajny,*[a] Anna M. Majcher,[b] Wojciech Nitek,[a] Michał Rams,[b] Elizaveta A. Suturina,[c] Liviu Ungur,[c] Liviu F. Chibotaru[c] and Barbara Sieklucka[a]

Received 29th August 2012,
Accepted 19th November 2012

DOI: 10.1039/c2ce26387d

www.rsc.org/crystengcomm

The novel layered $\{Co^{II}_3(2,2'\text{-bpdo})_4(H_2O)_4[W^{V}(CN)_8]_2\}\cdot 8H_2O$ (**1**) network (2,2′-bpdo = 2,2′-bipyridine-1,1′-dioxide) is built of 2-D corrugated cyanide-bridged brick-wall skeletons parallel to the *bc* crystallographic plane. The coordination of chelating 2,2′-bpdo to Co(II) gives 7-membered coordination rings. Magnetic and heat capacity measurements performed on monocrystalline samples reveal ferromagnetic ordering below T_C of 6 K. Magnetic anisotropy of the ordered phase is represented by the easy axis oriented in the *ac* crystallographic plane. Bulk magnetic anisotropy is confronted with a local anisotropy of Co complexes: a strong axial anisotropy of *trans,cis,cis*-$[Co^{II}(\mu\text{-}NC)_2(H_2O)_2(2,2'\text{-bpdo})]$ moieties represented by $g_x^{(2)} = 2.06$, $g_y^{(2)} = 2.95$ and $g_z^{(2)} = 7.30$, and a planar anisotropy of *trans,cis,cis*-$[Co^{II}(\mu\text{-}NC)_2(2,2'\text{-bpdo})_2]$ represented by $g_x^{(3)} = 5.40$, $g_y^{(3)} = 4.82$ and $g_z^{(3)} = 2.28$, determined by CASSCF/RASSI/SINGLE_ANISO *ab initio* calculations. The experimental data are explained by the molecular field simulation of the magnetic structure using the above theoretical data.

Introduction

Thriving progress in multifunctional magnetic coordination networks is owed to the judicious selection of the building blocks to create a specific molecular and intermolecular arrangement, which could result in the appearance of anticipated properties and function. The range of metal complexes of molecular/electronic ground state spin structures, responsive to the external physical or chemical stimulation, were explored for different types of functionality.[1,2] High spin cobalt(II) complexes offer flexible coordination number, internal magnetic anisotropy and distinct optical properties. These features establish their potential to form magnetically ordered phases,[3] low dimensional single-molecule magnets (SMMs)[4] or single chain magnets (SCMs),[5] spin–crossover complexes,[6] ferroelectric networks,[7] chiral systems,[8] guest sensitive dynamic networks[9] or thermally and optically driven phase transitions.[10]

The functional potential of cobalt(II,III)–octacyanidometalate(V,IV) compounds[11] has been recognized due to the magnetic studies of networks with long range ordering,[12] vapor sorption[13] and physical or chemical control of the equilibrium between different Co–$[W(CN)_8]^{n-}$ spin-state configurations.[12c,d,14] The attempts of description of the local magnetic anisotropy parameters or intermetallic exchange coupling parameters for these complexes are very rare,[12a,15,16] which is due to the non-trivial spin state diagrams of Co(II) complexes.[17] Several reports dealt with monocrystalline magnetism of M_A–$[M_B(CN)_8]^{n-}$ (M_A = Mn^{II}, Mn^{III}, Cu^{II}, Ln^{III}, M_B = W^{V}, Nb^{IV}),[18] while *none* of the Co^{II}–$[M^{V}(CN)_8]^{3-}$ compounds were investigated magnetically in the monocrystalline form.

Herein we present structural and magnetic monocrystalline characterisation of a novel layered network $\{Co^{II}_3(2,2'\text{-bpdo})_4(H_2O)_4[W^{V}(CN)_8]_2\}\cdot 8H_2O$ (**1**) (2,2′-bpdo = 2,2′-bipyridine-1,1′-dioxide) exhibiting long range ordering and magnetic anisotropy. The formation of a 2-dimensional network was achieved due to a relatively rare 2,2′-bpdo chelating arrangement, resulting in the $[M(bpdo)_x]^{n+}$ (M = 3d or 4f metal ions, x = 1–4, n = 2, 3) units capable to build polynuclear compounds with short distance intermetallic bridging,[19] porous chemical vapor sensitive systems[20] or luminescent complexes.[21]

Experimental

Materials

$Co^{II}Cl_2\cdot 6H_2O$, 2,2′-bpdo and solvents were purchased from commercial sources (Sigma Aldrich, Idalia) and used without

[a]*Faculty of Chemistry, Jagiellonian University, Ingardena 3, 30-060 Kraków, Poland. E-mail: podgajny@chemia.uj.edu.pl*
[b]*M. Smoluchowski Institute of Physics, Jagiellonian University, Reymonta 4, 30-059 Kraków, Poland*
[c]*Division of Quantum and Physical Chemistry, Katholieke Universiteit Leuven, Celestijnenlaan 200F, B-3001, Leuven, Belgium*

† Electronic supplementary information (ESI) available: X-ray crystallographic file in CIF format, deposition number: CCDC 834663; detailed metric parameters of **1**; supporting data for the description of magnetic properties of **1**; details of polyhedral shape analysis of **1**, details of *ab initio* calculations in PDF format, details of magnetic structure simulation. For ESI and crystallographic data in CIF or other electronic format see DOI: 10.1039/c2ce26387d

further purification. $Na_3[W^V(CN)_8]\cdot 4H_2O$ was synthesized according to the published procedure.[22]

Synthesis

0.3 mmol (72.4 mg) $CoCl_2\cdot 6H_2O$ and 0.3 mmol (56.9 mg) 2,2′-bpdo were dissolved together in 15 mL of the water : acetonitrile mixture (2 : 1, *v*/*v*) to give solution I. 0.3 mmol (160 mg) $Na_3[W(CN)_8]\cdot 2H_2O$ was dissolved in 10 mL of water to give solution II. Solutions I and II were stirred together for 30 minutes and after that were left in the dark for crystallization. After a month, dark red plate crystals of **1** suitable for X-ray measurements were collected, washed with water and air-dried. Yield: 90 mg, 47%. Elemental analysis. Found: C, 34.7%; H, 3.2%; N, 17.4%. Calc. for $C_{56}H_{64}Co_3N_{24}O_{20}W_2$: C, 34.7%; H, 3.3%; N, 17.3%. IR spectrum (KBr pellets) in cm^{-1}: ν(O–H), 3464s(br); ν(C≡N), 2187 w, 2169 m(sh), 2149 m(sh), 2137(w); $\delta(H_2O)$, 1610 s; 2,2′-bpdo, ν(ArC=C, ArC=N), 1559 w, 1478 s, 1443 m, 1425 s; ν(N–O), 1204 s; γ(ArCH), ring breathing, ring deformation, 1258 w, 1157 m, 1119 w, 1035 m, 848 s, 834 s, 771 s; coordination, 582 s, 526 m, 517 m, 467 m. TGA/QMS, line $q/m = 18^+$: 7.4% loss of total mass in *T* range 80–120 °C conforms to 8 crystallization H_2O; further 3.7% loss of total mass in *T* range 150–180 °C conforms to 4 coordination H_2O.

Crystal structure solution and refinement

Diffraction data for single crystal were collected on a Nonius KappaCCD four circle diffractometer, equipped with a Mo (0.71073 Å) Kα radiation source and graphite monochromator. Cell refinement and data reduction was performed using HKL SCALEPAC and DENZO.[23] Positions of non-hydrogen atoms were determined using SIR-97.[24] Refinement and further calculations were carried out using SHELXL-97.[25] The structure was solved by the heavy-atom Patterson method and refined through full-matrix least squares on F^2. The non-hydrogen atoms were refined anisotropically and the hydrogen atoms were refined isotropically. The positions of the hydrogen atoms in the water molecules were found on the basis of the linearity of the hydrogen bonds and were not refined. The selected crystallographic data are presented in Table 1.

Physical techniques

Elemental analyses (C, H, N) were performed using an EuroEA EuroVector elemental analyzer. Infrared spectra were measured in KBr pellets between 4000 and 400 cm^{-1} using a Bruker EQUINOX 55 FT-IR spectrometer. Thermogravimetric data in the temperature range 25–400 °C were collected on a mettler toledo TGA/SDTA 851e microthermogravimeter equipped with QMS Thermostar GSD 300 T Balzers at a heating rate of 10 °C min^{-1} in Ar atmosphere using positive ionisation. Magnetic measurements were performed using QuantumDesign SQUID magnetometer MPMS-XL. The powder magnetic signal was measured on the dry sample with mass 24.0(5) mg. Diamagnetic corrections were subtracted. Single crystal magnetic study was carried out on the chosen crystal with mass 1.00 mg. The heat capacity was measured using the QuantumDesign PPMS system in the range 2–200 K.

Table 1 Crystal data and structure refinement for **1**

Method	Single-crystal XRD
Empirical formula	$C_{28}H_{28}Co_{1.5}N_{12}O_{10}W$
Formula weight/g mol^{-1}	964.87
T/K	293(2)
λ/Å	0.71073
Crystal system	Monoclinic
Space group	$P2_1/c$
Unit cell dimensions/Å	a = 10.45700(10), b = 19.0970(2), c = 17.7070(5), $\alpha = \gamma = 90°$, β = 91.2120(10)°
V/Å^3	3535.25(6)
Z	4
D_{calc}/g cm^{-3}	1.813
μ/mm^{-1}	4.018
F(000)	1898
Crystal size/mm × mm × mm	0.1 × 0.25 × 0.45
Θ range for data collection/°	2.89 to 27.48
Limiting indices	$-13 < h < 13$, $-24 < k < 24$, $-22 < l < 22$
Reflections collected/unique [R_{int}]	29 931/8100 [0.0389]
Completeness to Θ_{max}/%	99.7
Absorption correction	Semi-empirical form equivalents
Max. and min. transmission	0.6894 and 0.2650
Refinement method	Full-matrix least-squares of F^2
Data/restraints/parameters	8100/0/475
Goodness-of-fit on F^2	1.036
Final R indices [$I > 2\sigma(I)$]	R_1 = 0.028, wR_2 = 0.0717
R indices (all data)	R_1 = 0.0376, wR_2 = 0.075
Largest diff. peak and hole	1.044 and −0.918 e Å^{-3}

Ab initio calculations

All *ab initio* calculations were performed with the MOLCAS 7.6 program package.[26] Suitable fragments containing only one magnetic center were built in order to study local electronic and magnetic properties of the Co2 and Co3 sites. Neighboring W metal sites were computationally replaced by diamagnetic Ta. The structure of the calculated fragments is shown in the ESI† (see Fig. S3 and S4). The basis sets describing individual atoms were taken from the ANO-RCC[27] and ANO-DK3[28] basis set libraries available in standard MOLCAS distribution. Contractions of the employed basis sets are shown in the ESI† (see Table S6). The Cholesky decomposition of the bielectronic integrals was employed in order to reduce the computational time.[26] Threshold of the Cholesky decomposition was 1.0×10^{-5}.

Relativistic effects were taken into account in two steps, both based on the Douglas–Kroll Hess Hamiltonian.[29] Scalar relativistic effects were included in the generation of the basis set describing individual atoms, which were further used within the complete active space self consistent field (CASSCF) method[30] for the determination of the low-lying spin states (quartets and doublets, in the case of Co^{2+}). The first active space of the CASSCF method, denoted AS1, included seven electrons in five orbitals (the 3d shell of the Co^{2+} ion). In order to account for the double shell effect,[31] a second shell of five empty d orbitals was added to the initial active space, giving an active space of seven electrons in ten orbitals (AS2). In the second step, the spin–orbit coupling was considered in the atomic mean field (AMFI) approximation, within the restricted active space state interaction (RASSI)[32] method, which uses the

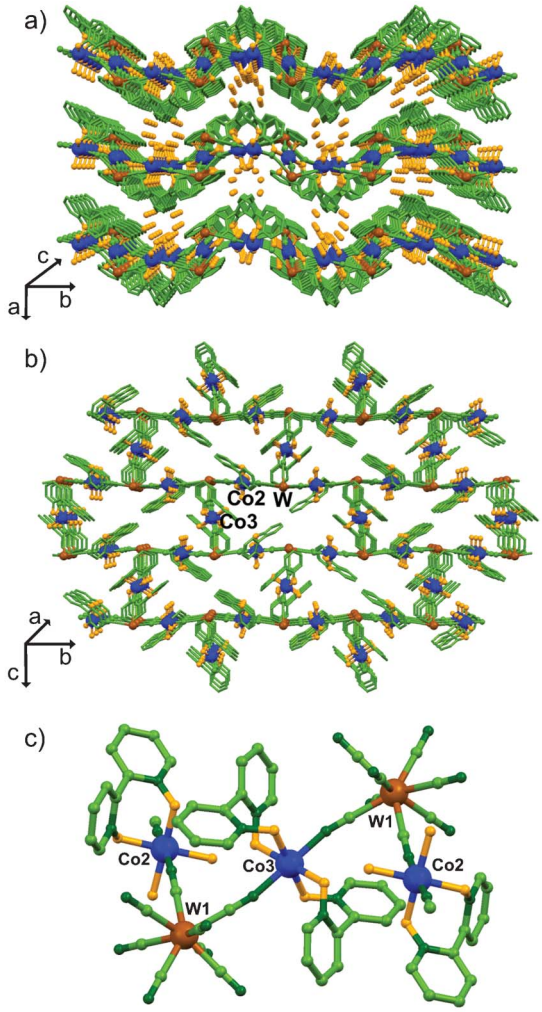

Fig. 1 The crystal structure of **1**: (a) projection along the *c* axis, (b) projection on the *bc* plane and (c) representative molecular fragment. Colors: Co(II) (dark blue), W(V) (brown), C and N (green), O (yellow). Hydrogen atoms (a–c) and crystallized water molecules are omitted for clarity (b, c).

roots of the CASSCF wave function as input states. In the present case of Co^{2+} ($3d^7$ electronic configuration), 10 quartet spin states and 40 doublet spin states were mixed by the spin–orbit coupling in RASSI, giving rise to 120 spin–orbital states. Finally, the magnetic properties of the low-lying Kramers doublets were computed by the module SINGLE_ANISO,[33,34] available in MOLCAS 7.6.

Results and discussion

Crystal structure

The crystal structure of **1** is presented in Fig. 1 and 2 and Fig. S1, ESI.† It is composed of CN^--bridged corrugated layers parallel to the *bc* plane and crystallized H_2O molecules between them. The layers reveal the canonical brick wall topology and consist of 36-membered rings with alternate Co^{II} and W^V centers connected through CN^- bridges. The geometry of the Co_6W_6 rings is close to deformed rectangles with dimensions of 19.1 × 10.3 $Å^2$. The metric parameters of the W and Co moieties are within the ranges typical for this class of compounds (ESI,† Table S1). $[W^V(CN)_8]^{3-}$ units have geometries close to ideal SAPR-8 geometries[35] with the C_4 axis close to the *a* crystallographic direction. Each $[W(CN)_8]^{3-}$ is linked to three Co^{II} moieties of distorted octahedral geometry (ESI,† Tables S2–S4):[35] two *trans,cis,cis*-[Co(2)(μ-NC)$_2$(H$_2$O)$_2$(bpdo)] along the *b* direction and one *trans,cis,cis*-[Co(3)(μ-NC)$_2$(bpdo)$_2$] along the *c* direction. The coordination of 2,2′-bpdo to Co(II) centers leads to the 7 membered coordination rings (Co–O–N–C–C–N–O–).[19–21] The W–C–N and Co–N–C angles in the bridging linkages are close to 180° with the exception of the angle Co2–N12–C12 being equal to 154.5°. Co–W distances are 5.30, 5.36 and 5.44 Å. The interlayer hydrogen bonds between terminal cyano ligands and water molecules lead to a supramolecular 3-D architecture, while the intra-layer π–π stacking system composed of aromatic parts of 2,2′-bpdo stabilizes the coordination skeleton (Fig. 2). The most significant hydrogen bonds, O1–H···N15 and O1–H···N18, lead to the formation of 16-centered rings described by graph-set analysis as a $R_4^2(16)$ motif.[36] The layer thickness along the *a* direction is about 8 Å, while the shortest distance between metallic centers of neighboring layers is 9.5 Å (W1···Co3).

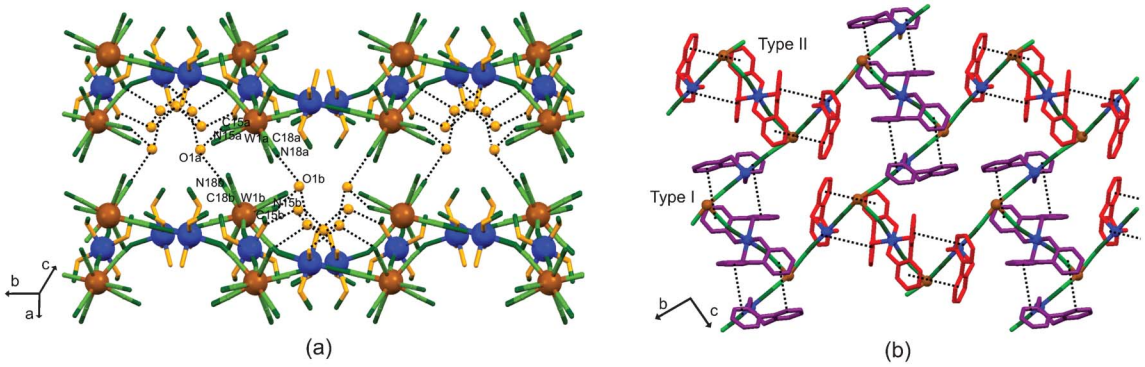

Fig. 2 Non-covalent interactions in **1**: (a) hydrogen bonds and (b) π–π stacking along the [011] axis (Type I) and [01-1] axis (Type II). Colors: Co(II) (dark blue), W(V) (brown), carbon atoms (green), nitrogen atoms (dark green), oxygen atoms (yellow), type I π–π interactions (violet), type II π–π interactions (red).

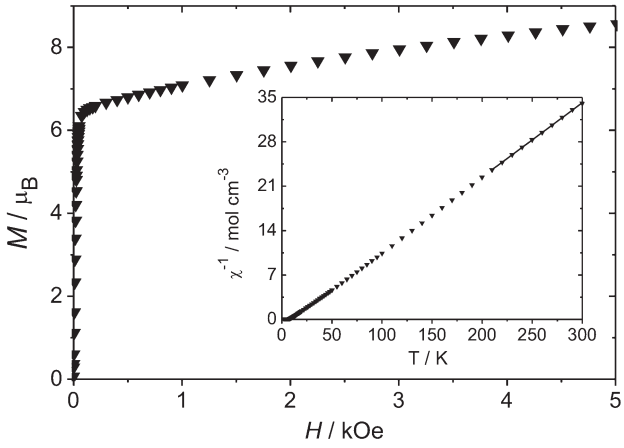

Fig. 3 $M(H)$ dependence (T = 2 K) and $\chi^{-1}(T)$ dependence (H = 1 kOe) for powder of **1** (inset) with the best fit to Curie–Weiss law (line).

Magnetic properties

The inverse magnetic susceptibility measured for a powder sample at H = 1 kOe is presented in Fig. 3. The Curie–Weiss law was fitted to the data in the temperature range 210–300 K. The Curie constant obtained from the fit of C = 8.54(4) K cm^3 mol^{-1} is very close to the low limit of the range 8.83–10.93 K cm^3 mol^{-1} expected for the W_2Co_3 unit in **1**, assuming the 2.7–3.4 range for octahedral high-spin Co(II) complexes[17], s_W=1/2 and g_W = 1.97.[37] The positive Weiss temperature Θ = 8.4 K indicates a predominant ferromagnetic coupling. $M(H)$ dependence for powder samples is shown in Fig. 3. Starting from the zero magnetic field it increases rapidly reaching 6.5 μ_B at H = 300 Oe and then continues to increase slowly reaching 8.7 μ_B at 50 kOe without saturation (per Co_3W_2 unit), which corresponds well to the relevant data measured for other cyanido-bridged $Co^{II}{}_3W^{V}{}_2$ or $Co^{II}{}_2Nb^{IV}$ networks (ESI,† Table S5).[12a,d,e,18f]

Fig. 4 presents the field cooling magnetisation curves for the single crystal sample measured for $H||a$ in various fields. A

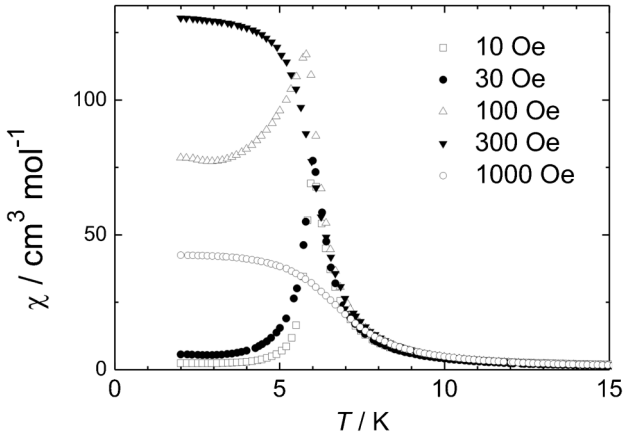

Fig. 4 Magnetic field cooling susceptibility *versus* temperature of a single crystal sample measured for $H||a$ axis in various fields.

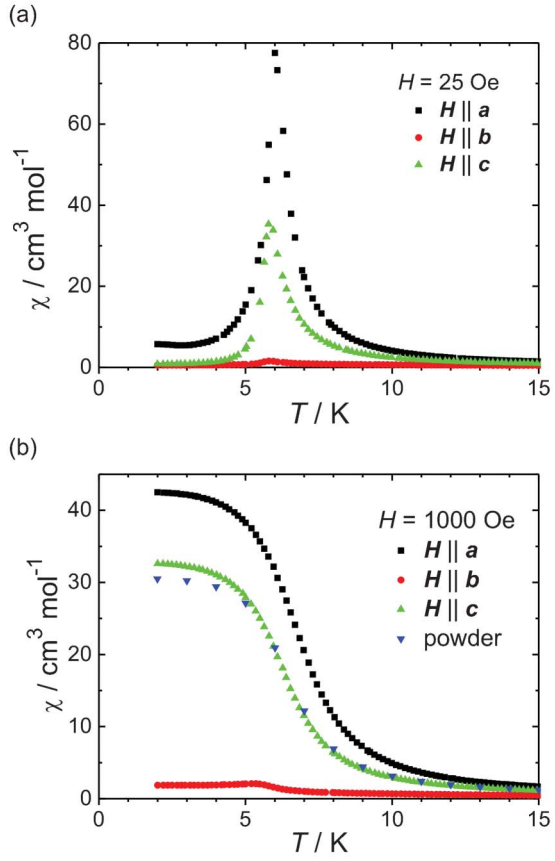

Fig. 5 Magnetic field cooling susceptibility *versus* temperature of a single crystal sample *versus* temperature measured for three crystallographic directions at H = 25 Oe (a) and at H = 1000 Oe (b).

switching of the magnetization from antiferro- to ferromagnetic is clearly seen in higher fields. Fig. 5 shows the magnetic susceptibility *versus* temperature of a single crystal sample measured along three crystallographic directions at H = 25 Oe and at H = 1000 Oe. From these curves we can also obtain the transition temperature of 5.9 K. The ordering is confirmed by the *ac* characteristics (Fig. S2, ESI†). The signal induced along the *b* axis indicates that this direction is very close to a bulk hard axis of magnetization. The easy magnetization axis could not be anticipated from the signals along the *a* and *c* axes. To clarify this, the measurements of the magnetic moment of a single crystal sample at T = 2 K and H = 1000 Oe *versus* the rotation position were performed, with the sample rotated around the *b* axis (Fig. 6). The expression $|M_S\sin(\delta - \delta_0)|$ was fitted to the data, marked as the solid line in Fig. 6. The easy magnetization axis (the maximum of the curve in Fig. 6) creates the angle of 39(1)° with the *a* axis, which was also checked by aligning the sample along the hard axis and measuring this angle after removing the crystal from the magnetometer. The minima on the curve in Fig. 6 indicate the presence of the hard direction in the *ac*-plane at an angle of 129° in respect to the *a* axis.

Fig. 7 shows magnetization *versus* field measured along the easy and hard magnetization axes in the *ac* plane and along the *b* crystallographic axis. For the data measured at the

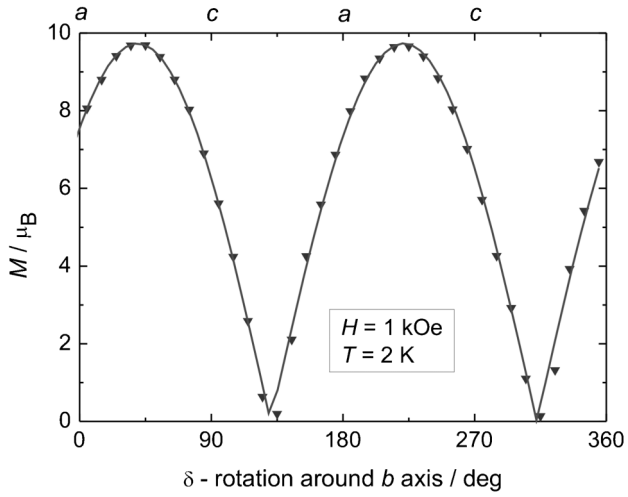

Fig. 6 Magnetization measured at T = 2 K and H = 1000 Oe for single crystal of **1** rotated around the *b* crystallographic axis. The line represents the fit (see text).

H||easy axis the magnetization saturates rapidly at the value close to 10 μ_B. The inset in Fig. 7 shows a hysteresis loop for the H||easy magnetization axis, revealing a spin–flip transition at around 100 Oe, which is consistent with the field-cooling curves from Fig. 4. A small coercive field is observed.

Summarizing the presented magnetic measurements, the magnetic structure of **1** in the zero field consists of antiferromagnetically coupled layers of Co(II) and W(V) magnetic moments interacting through cyanide-bridges, each layer having a non-zero magnetic component along the determined easy axis. In the ordered structure below 6 K a large magnetic anisotropy is present with the effective anisotropy field H_A estimated to be 100 kOe at 1.8 K. This can be interpreted in terms of single ion anisotropy of Co(II) ions[38] resulting in a preference of their magnetic moments to align along their easy anisotropy axes (see *Ab initio calculations* section).

The data in Fig. 7 indicate that the field of 1 kOe is both, sufficiently high to overcome the intra-layer interaction and sufficiently low to make the measurements of magnetic moment *versus* rotation position possible (Fig. 6), and well described by the $|M_s\sin(\delta)|$.

The heat capacity of the sample comprising several monocrystalline grains of **1** was measured by the relaxation method. The sharp λ-shaped peak observed at 5.7 K corresponds to the second order transition to the ordered state observed in magnetic measurements of **1** below 5.9 K. The phonon contribution was subtracted using the Debye model fit to the data in the limited range 27–40 K. The remaining magnetic contribution C_{mag} to heat capacity is shown in Fig. 8. The magnetic entropy gain calculated as an integral of C_{mag}/T in the range 2 to 25 K is S_m = 26 J K^{-1} mol^{-1}. This value is consistent with expected 28.8 J K^{-1} mol^{-1} calculated from the relation $S = R\ln(2s + 1)$, for the set of 3 Co(II) spins with s_{Co}^{LT} = 1/2 in the ground state expected at low temperature (LT) and 2 W(V) spins with s_W = 1/2. It can be seen in Fig. 8 that most of the entropy is gained above the transition temperature, which is characteristic for low-dimensional ferromagnets. These results are consistent with the results of magnetic measurements and with the structural properties of **1**.

Ab initio calculations

To explain the bulk magnetic anisotropy we performed the *ab initio* calculations of local anisotropy axes of Co(II) centers on individual Co centers for trinuclear cyanide-bridged fragments $[Ta(CN)_8]_2Co(2,2'\text{-bpdo})(H_2O)_2]$ (Co2) (Fig. S3, ESI†) and $[Ta(CN)_8]_2Co(2,2'\text{-bpdo})_2]$ (Co3) (Fig. S4, ESI†), where the diamagnetic Ta^{5+} ions substituted the paramagnetic W^{5+} ions. The obtained energies of the spin states for Co2 and Co3 centers are shown in Tables S7 and S8, ESI,† respectively. The electronic configuration of the Co^{2+} is $3d^7$, while the ground ionic multiplet for an octahedral ligand field environment is $^4T_1$. The deviation from an ideal octahedral symmetry leads to a splitting of the orbital degeneracy of the ground orbital triplet $^4T_1$. As we can see in Tables S7 and S8, ESI,† the total

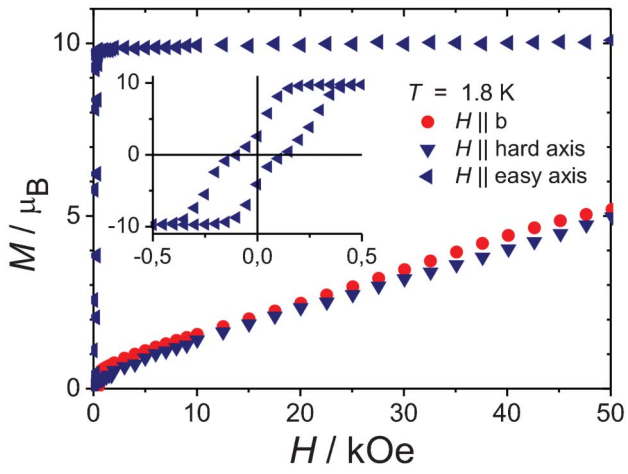

Fig. 7 Magnetization of a single crystal sample measured at T = 1.8 K along the *b* crystallographic axis, and two directions in the *ac* plane: the hard and easy magnetization axis. Inset: hysteresis loop for the easy magnetization axis revealing a spin–flip transition at around 100 Oe.

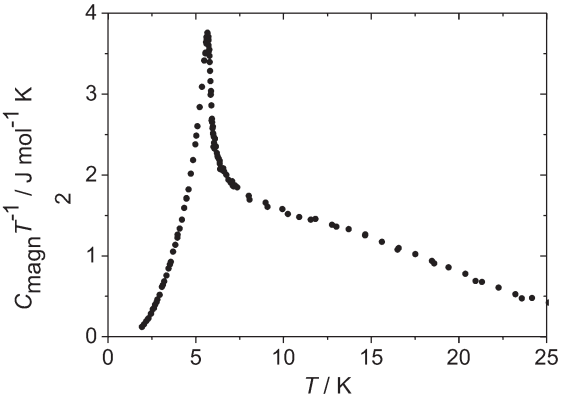

Fig. 8 Magnetic contribution of the heat capacity for **1**.

energy splitting of the ground orbital triplet $^4T_1$ (marked yellow) is similar (approx. 1230 cm^{-1}) for both Co2 and Co3 centers, while their splitting patterns are very different: it is almost equidistant in Co2, while in Co3 it is almost of the ^4A + ^4E type. This effect is due to the structural differences between Co2 and Co3 sites which strongly influence the spin–orbit coupling: the mixing of the low-lying quartet spin states is smaller in Co3 than in Co2, and as a result, the magnetic anisotropy of the ground Kramers doublet is completely different: magnetic anisotropy in Co3 is weaker than in Co2. The resulting energy differences between the ground Kramers doublet and the first excited Kramers doublet are in agreement with the values found for 6-coordinated Co(II) complexes.[39] The representative g_x, g_y, and g_z trace elements of the g tensor are presented in Table 2. The graphical representation is shown in Fig. 9 in the top panel.

The Co2 centers reveal a strong axial anisotropy with the easy $g_z^{(2)}$ axis oriented almost parallel to the axial CN–Co–NC direction of the $[Co(\mu\text{-}NC)_2(2,2'\text{-bpdo})(H_2O)_2]$ units, and close to b crystallographic directions. The hard $g_x^{(2)}$ and $g_y^{(2)}$ axes are close to the diagonals of the equatorial plane of this complexes. The Co3 centers reveal a planar anisotropy with a hard $g_z^{(3)}$ component parallel to the [111] direction of $[Co(\mu\text{-}NC)_2(2,2'\text{-bpdo})_2]$ units and close to the b crystallographic directions. Such orientation of g_x, g_y and g_z directions is consequently propagated through the whole structure due to the symmetry elements of inversion centers, glide planes and 2-fold proper axes within the regime of space group $P2_1/c$.

Magnetic structure simulation

The magnetic structure was simulated within the molecular field approach. The energy of the set of magnetic moments in the molecular field was minimized to calculate magnetic moments in the ordered structure. The g-tensors and their orientations determined by the *ab initio* calculations were used for Co ions, while the isotropic g-tensor for W was assumed. To calculate magnetic moments we considered solely the orientation of the molecular field at different sites in the saturation limit at T = 0 K. The identical ferromagnetic W–Co interaction was additionally assumed for all Co2–W and Co3–W pairs. The details of the simulation with the equations used and numerical results are enclosed in ESI.† The obtained magnetic structure is presented in Fig. 9 in the bottom panel. The calculated spontaneous magnetization along the easy direction is 9.75 μ_B, while the magnetization values along the crystallographic axes are M_a = −8.76, M_{b^*} = 0.0, M_c = 4.28 μ_B, all per Co_3W_2 unit. The magnetization easy axis is oriented in the *ac* plane, forming the angle of 26° with the *a* crystallographic axis. The magnetization cancels along the $b^* \approx b$ direction. The above simulation accurately explains both the value of magnetization and the easy axis direction measured experimentally. It is worth noting, that due to competing anisotropies of Co2 and Co3 ions, the magnetic moments of Co2 are far from the local easy axis of Co2.

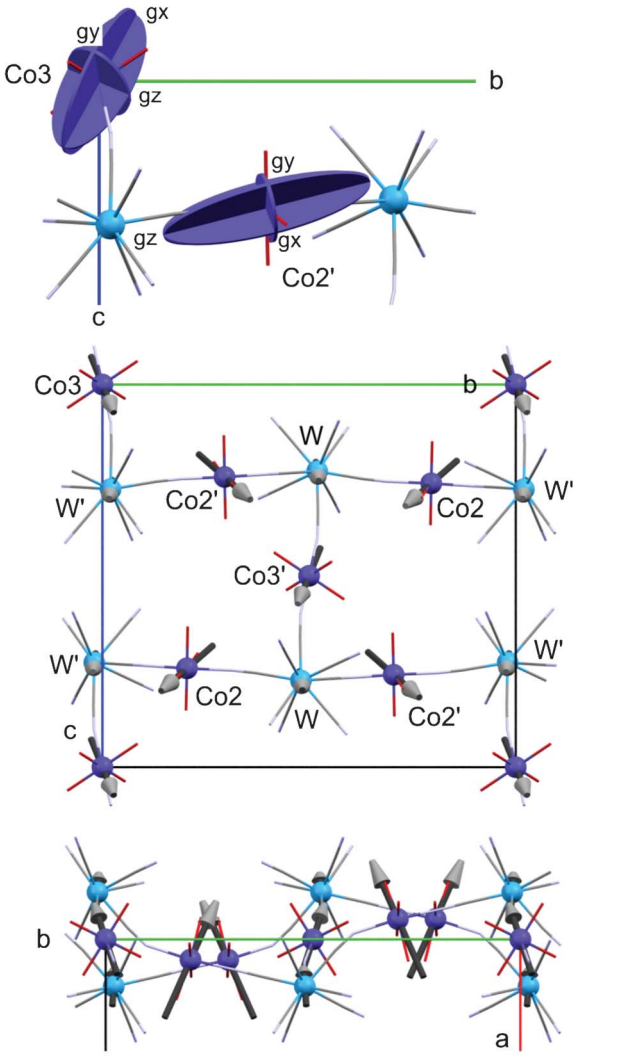

Fig. 9 (Top) Graphical representations of g tensor together with the crystallographic direction. g-tensors for primed and non-primed Co ions differ only by orientation. (Middle) Magnetic structure obtained from the total energy minimization, viewed along the *a* axis. The length of the magnetic moment is scaled as 0.5μ_B/Å. (Bottom) Magnetic structure of single layer viewed along the *c* axis.

Table 2 Energies (cm^{-1}) and g tensors of the lowest Kramers doublets (KD)

		AS1		AS2	
		E/cm^{-1}	g	E/cm^{-1}	g
Co2					
1	g_x	0.000	2.0614	0.000	1.9463
	g_y		2.9498		2.7973
	g_z		7.3014		7.3166
2	g_x	172.535	1.8195	150.650	1.9356
	g_y		1.9709		2.0158
	g_z		5.5358		5.5448
Co3					
1	g_x	0.000	5.3965	0.000	5.1363
	g_y		4.8190		4.9199
	g_z		2.2831		2.2374
2	g_x	112.973	0.2423	93.294	0.0835
	g_y		0.2922		0.1208
	g_z		6.2344		6.2483

The final image of the magnetism in the ordered layers would be provided by neutron diffraction experiments and by the magnetic structure solution and refinement including calculation of exchange coupling constant J_{WCo}.

Conclusions

A novel layered cyano-bridged Co(II)–W(V) molecular magnet with rare $[Co^{II}(2,2'\text{-bpdo})_x]$ (x = 1 and 2) chelate units exhibits a strong magnetic anisotropy in the ferromagnetically ordered phase below a T_C of 6 K. The bulk magnetic anisotropy is correlated with the anisotropy of the g tensor (g_x, g_y and g_z) of ground Kramers doublets of the Co(II) magnetic centers. It was found that two different types of the local magnetic anisotropy are present in **1**: a strong axial anisotropy for $[Co(NC)_2(2,2'\text{-bpdo})(H_2O)_2]$ and a planar anisotropy for $[Co(NC)_2(2,2'\text{-bpdo})_2]$ moieties. The bulk magnetic anisotropy with one well distinguished easy direction is the result of combined effects of local Co(II) anisotropy, which is simulated within the molecular field approach. The structural modifications of the layered $\{Co^{II}_3(2,2'\text{-bpdo})_4(H_2O)_4[W^V(CN)_8]_2\}\cdot 8H_2O$ (**1**) network towards polar or chiral species may open a pathway towards multifunctional layered magnetic systems.

Acknowledgements

This work was partially supported by the Polish Ministry of Science and Higher Education within Research Projects 1535/B/H03/2009/36, by the Polish National Science Centre (Grant UMO-2011/01/B/ST5/00716), and by the International PhD-studies Programme at the Faculty of Chemistry, Jagiellonian University, within the Foundation for Polish Science MPD Programme (S. Chorazy) co-financed by the EU European Regional Development Fund. The research was partially carried out with the equipment purchased thanks to the financial support of the European Regional Development Fund in the framework of the Polish Innovation Economy Operational Program (contract no. POIG.02.01.00-12-023/08). L. Ungur is a post-doctoral fellow of the FWO-Vlanderen (Fonds voor Wetenschappelijk Onderzoek-Vlanderen). E. A. Suturina and L. Ungur gratefully acknowledge the financial support from the *INPAC* and *Methusalem* grants of the KU Leuven. E.A.S. also appreciates the support of this work by the Russian Ministry of Education and Science (project 2012-1.3.2-12-000-1012, contract 14.132.21.1451), Mikhail Prokhorov and Zamaraev Foundations.

References

1 (*a*) S. R. Batten, S. M. Neville and D. Turner, *Coordination Polymers: Design, Analysis and Applications*, The Royal Society of Chemistry, Cambridge, 2009; (*b*) O. Sato, J. Tao and Y.-Z. Zhang, *Angew. Chem., Int. Ed.*, 2007, **46**, 2152–2187; (*c*) E. Pardo, R. Ruiz-García, J. Cano, X. Ottenwaelder, R. Lescouëzec, R. Y. Journaux, F. Lloret and M. Julve, *Dalton Trans.*, 2008, 2780–2805; (*d*) M. Andruh, J.-P. Costes, C. Diaz and S. Gao, *Inorg. Chem.*, 2009, **48**, 3342–3359.

2 (*a*) M. Clemente-León, E. Coronado, C. Martí-Gastaldo and F. M. Romero, *Chem. Soc. Rev.*, 2011, **40**, 473–497; (*b*) G. Férey, C. Serre, T. Devic, G. Maurin, H. Jobic, P. L. Llewellyn, G. De Weireld, A. Vimont, M. Daturi and J.-S. Chang, *Chem. Soc. Rev.*, 2011, **40**, 550–562; (*c*) J. Rocha, L. D. Carlos, F. A. A. Paz and D. Ananias, *Chem. Soc. Rev.*, 2011, **40**, 926–940; (*d*) O. Shekhah, J. Liu, R. A. Fischer and C. Wöll, *Chem. Soc. Rev.*, 2011, **40**, 1081–1106; (*e*) J. A. A. W. Elemans, S. Lei and S. De Feyter, *Angew. Chem., Int. Ed.*, 2009, **48**, 7298–7332.

3 (*a*) E. Coronado, J. R. Galan-Mascaros and C. Martí-Gastaldo, *Inorg. Chem.*, 2007, **46**, 8108–8110; (*b*) R.-Y. Li, X.-Y. Wang, T. Liu, H.-B. Xu, F. Zhao, Z.-M. Wang and S. Gao, *Inorg. Chem.*, 2008, **47**, 8134–8142; (*c*) N. Marino, T. F. Mastropietro, D. Armentano, G. De Munno, R. P. Doyle, F. Lloret and M. Julve, *Dalton Trans.*, 2008, 5152–5154; (*d*) P. Mahata, S. Natarajan, P. Panissod and M. Drillon, *J. Am. Chem. Soc.*, 2009, **131**, 10140–10150.

4 M. Murrie, *Chem. Soc. Rev.*, 2010, **39**, 1986–1995.

5 H.-L. Sun, Z.-M. Wang and S. Gao, *Coord. Chem. Rev.*, 2010, **254**, 1081–1100.

6 S. Hayami, R. Moriyama, A. Shuto, Y. Madea, K. Ohta and K. Inoue, *Inorg. Chem.*, 2007, **46**, 7692–7694.

7 (*a*) C. Livage, N. Guillou, P. Rabu, P. Pattison, J. Marrot and G. Ferey, *Chem. Commun.*, 2009, 4551–4553; (*b*) N. Ohta, A. Fuyuhiro and K. Yamanari, *Inorg. Chem.*, 2010, **49**, 9122–9124; (*c*) X. Liu, Y. Xing, X. Wang, H. Xu, X. Liu, K. Shaoa and Z. Su, *Chem. Commun.*, 2010, **46**, 2614–2616; (*d*) E. Pardo, C. Train, R. Lescouëzec, Y. Journaux, J. Pasán, C. Ruiz-Pérez, F. Delgado, R. Ruiz-Garcia, F. Lloret and C. Paulsen, *Chem. Commun.*, 2010, **46**, 2322–2324.

8 (*a*) O. Sengupta and P. S. Mukherjee, *Inorg. Chem.*, 2010, **49**, 8583–8590; (*b*) Y.-Z. Zhang and O. Sato, *Inorg. Chem.*, 2010, **49**, 1271–1273.

9 (*a*) L. G. Beauvais, M. P. Shores and J. R. Long, *J. Am. Chem. Soc.*, 2000, **122**, 2763–2772; (*b*) D. Bradshaw, J. E. Warren and M. J. Rosseinsky, *Science*, 2007, **315**, 977–980; (*c*) M.-H. Zeng, S. Hu, Q. Chen, G. Xie, Q. Shuai, S.-L. Gao and L.-Y. Tang, *Inorg. Chem.*, 2009, **48**, 7070–7079; (*d*) L. Robertson, M. Duttine, M. A. Gaudon and A. Demourgues, *Chem. Mater.*, 2011, **23**, 2419–2427.

10 (*a*) D. Li, R. Clérac, O. Roubeau, E. Harté, C. Mathonière, R. Le Bris and S. M. Holmes, *J. Am. Chem. Soc.*, 2008, **130**, 252–258; (*b*) Y. Zhang, D. Li, R. Clérac, M. Kalisz, C. Mathonière and S. M. Holmes, *Angew. Chem., Int. Ed.*, 2010, **49**, 3752–3756; (*c*) C. Avendano, M. G. Hilfiger, A. Prosvirin, C. Sanders, D. Stepien and K. R. Dunbar, *J. Am. Chem. Soc.*, 2010, **132**, 13123–13125; (*d*) M. Ohba, K. Yoneda and S. Kitagawa, *CrystEngComm*, 2010, **12**, 159–165.

11 (*a*) B. Sieklucka, R. Podgajny, T. Korzeniak, B. Nowicka, D. Pinkowicz and M. Kozieł, *Eur. J. Inorg. Chem.*, 2011, 305–326; (*b*) B. Nowicka, T. Korzeniak, O. Stefańczyk, D. Pinkowicz, S. Chorazy, R. Podgajny and B. Sieklucka, *Coord. Chem. Rev.*, 2012, **256**, 1946–1971.

12 (*a*) J. M. Herrera, A. Bleuzen, Y. Dromzee, M. Julve, F. Lloret and M. Verdaguer, *Inorg. Chem.*, 2003, **42**, 7052–7059; (*b*) D. Li, L. Zheng, Y. Zhang, J. Huang, S. Gao and W. Tang,

Inorg. Chem., 2003, **42**, 6123–6129; (*c*) Y. Arimoto, S. Ohkoshi, Z. J. Zhong, H. Seino, Y. Mizobe and K. Hashimoto, *J. Am. Chem. Soc.*, 2003, **125**, 9240–9241; (*d*) S. Ohkoshi, Y. Hamada, T. Matsuda, Y. Tsunobuchi and H. Tokoro, *Chem. Mater.*, 2008, **20**, 3048–3054; (*e*) R. Podgajny, M. Bałanda, M. Sikora, M. Borowiec, L. Spałek, C. Kapusta and B. Sieklucka, *Dalton Trans.*, 2006, 2801–2809.

13 (*a*) S. Willemin, J. Larionova, R. Clérac, B. Donnadieu, B. Henner, X. F. Le Goff and Ch. Guérin, *Eur. J. Inorg. Chem.*, 2003, 1866–1872; (*b*) R. Podgajny, S. Chorazy, W. Nitek, A. Budziak, M. Rams, J. C. Gomez-García, M. Oszajca, W. Łasocha and B. Sieklucka, *Cryst. Growth Des.*, 2011, **11**, 3866–3876.

14 (*a*) T. Mahfoud, G. Molnár, S. Bonhommeau, S. Cobo, L. Salmon, P. Demont, H. Tokoro, S. Ohkoshi, K. Boukheddaden and A. Bousseksou, *J. Am. Chem. Soc.*, 2009, **131**, 15049–15054; (*b*) M. Kozieł, R. Podgajny, R. Kania, R. Lebris, C. Mathonière, K. Lewiński, K. Kruczała, M. Rams, C. Labrugère, A. Bousseksou and B. Sieklucka, *Inorg. Chem.*, 2010, **49**, 2765–2772.

15 S. Clima, M. F. A. Hendrickx, L. F. Chibotaru, A. Soncini, V. Mironov and A. Ceulemans, *Inorg. Chem.*, 2007, **46**, 2682–2690.

16 D. Pinkowicz, R. Pełka, O. Drath, W. Nitek, M. Bałanda, A. M. Majcher, G. Poneti and B. Sieklucka, *Inorg. Chem.*, 2010, **49**, 7565–7576.

17 F. Lloret, M. Julve, J. Cano, R. Ruiz-García and E. Pardo, *Inorg. Chim. Acta*, 2008, **361**, 3432–3445.

18 (*a*) Y. Song, S. Ohkoshi, Y. Arimoto, H. Seino, Y. Mizobe and K. Hashimoto, *Inorg. Chem.*, 2003, **42**, 1848–1856; (*b*) P. Przychodzen, K. Lewinski, M. Bałanda, R. Pełka, M. Rams, T. Wasiutynski, C. Guyard-Duhayon and B. Sieklucka, *Inorg. Chem.*, 2004, **43**, 2967–2974; (*c*) P. Przychodzeń, R. Pełka, K. Lewiński, J. Supel, M. Rams, K. Tomala and B. Sieklucka, *Inorg. Chem.*, 2007, **46**, 8924–8938; (*d*) M. Bałanda, R. Pełka, T. Wasiutyński, M. Rams, Y. Nakazawa, Y. Miyazaki, M. Sorai, R. Podgajny, T. Korzeniak and B. Sieklucka, *Phys. Rev. B: Condens. Matter Mater. Phys.*, 2008, **78**, 174409; (*e*) D. Pinkowicz, R. Podgajny, W. Nitek, M. Rams, A. M. Majcher, T. Nuida, S. Ohkoshi and B. Sieklucka, *Chem. Mater.*, 2011, **23**, 21–31; (*f*) D. Pinkowicz, M. Rams, W. Nitek, B. Czarnecki and B. Sieklucka, *Chem. Commun.*, 2012, **48**, 8323–8325.

19 G. A. van Albada, I. Mutikainen, U. Turpeinen and J. Reedijk, *Polyhedron*, 2007, **26**, 2728–2732.

20 G. Zheng, Y. Y. Li, H.-D. Guo, S. Y. Song and H.-J. Zhang, *Chem. Commun.*, 2008, 4918–4920.

21 E. Huskowska, I. Turowska-Tyrk, J. Legendziewicz and J. P. Riehl, *New J. Chem.*, 2002, **26**, 1461–1467.

22 A. Samotus, *Pol. J. Chem.*, 1973, **47**, 653–657.

23 Z. Otwinowski and W. Minor, *Methods in Enzymology, Macromolecular Crystallography, Part A*, ed. C. W. Carter Jr and R. M. Sweet, Academic Press, New York, 1997, vol. 276, pp. 307–326.

24 M. Altomare, M. C. Burla, M. Camalli, G. L. Cascarano, C. Giacovazzo, A. Guagliardi, A. G. G. Moliterni, G. Polidori and R. Spagna, *J. Appl. Crystallogr.*, 1999, **32**, 115–119.

25 G. M. Sheldrick, *Acta Crystallogr., Sect. A: Found. Crystallogr.*, 2008, **64**, 112–122.

26 F. Aquilante, L. De Vico, N. Ferré, G. Ghigo, P.-A. Malmqvist, P. Neogrády, T. B. Pedersen, M. Pitoňák, M. Reiher, B. O. Roos, L. Serrano-Andrés, M. Urban, V. Veryazov and R. Lindh, *J. Comput. Chem.*, 2010, **31**, 224–247.

27 (*a*) B. O. Roos, R. Lindh, P.-A. Malmqvist, V. Veryazov and P.-O. Widmark, *J. Phys. Chem. A*, 2005, **108**, 2851–2858; (*b*) B. O. Roos, R. Lindh, P.-A. Malmqvist, V. Veryazov and P. O. Widmark, *J. Phys. Chem. A*, 2005, **109**, 6575–6579.

28 T. Tsuchiya, M. Abe, T. Nakajima and K. Hirao, *J. Chem. Phys.*, 2001, **115**, 4463–4472.

29 B. A. Hess, C. M. Marian, U. Wahlgren and O. Gropen, *Chem. Phys. Lett.*, 1996, **251**, 365–371.

30 B. O. Roos and P.-A. Malmqvist, *Phys. Chem. Chem. Phys.*, 2004, **6**, 2919–2927.

31 K. Andersson and B. O. Roos, *Chem. Phys. Lett.*, 1992, **191**, 507–514.

32 P.-A. Målmqvist, B. O. Roos and B. Schimmelpfennig, *Chem. Phys. Lett.*, 2002, **357**, 230–240.

33 L. Ungur and L. F. Chibotaru, *The computer program SINGLE_ANISO*, University of Leuven, 2006–2012.

34 L. F. Chibotaru and L. Ungur, *J. Chem. Phys.*, 2012, **137**, 064112.

35 (*a*) D. Visinescu, C. Desplanches, I. Imaz, V. Bahers, R. Pradhan, F. A. Villamena, P. Guionneau and J.-P. Sutter, *J. Am. Chem. Soc.*, 2006, **128**, 10202–10212; (*b*) M. Llunell, D. Casanova, J. Cirera, M. P. Alemany and S. Alvarez, *SHAPE, v. 2.0, Program for the Stereochemical Analysis of Molecular Fragments by Means of Continuous Shape Measures and Associated Tools, Departament de Química Física, Departament de Química Inorganica, and Institut de Química Teorica i Computacional*, Universitat de Barcelona, Barcelona, Spain, 2010.

36 J. Bernstein, R. E. Davis, L. Shimoni and N.-L. Chang, *Angew. Chem., Int. Ed. Engl.*, 1995, **34**, 1555–1573.

37 P. M. Kiernan and W. P. Griffith, *J. Chem. Soc., Dalton Trans.*, 1975, 2489–2494.

38 (*a*) R. Boča, *Coord. Chem. Rev.*, 2004, **248**, 757–815; (*b*) B. Papankova, R. Boča, L. Dlhan, I. Nemec, J. Titiš, I. Svoboda and H. Fuess, *Inorg. Chim. Acta*, 2010, **363**, 147–156; (*c*) J. Titiš and R. Boča, *Inorg. Chem.*, 2010, **49**, 3971–3973; (*d*) R. E. Greeney, C. P. Landee, J. H. Zhang and W. M. Reiff, *Phys. Rev. B*, 1989, **39**, 12200–12214; (*e*) E. J. Kinast, C. A. dos Santos, D. Schmitt, O. Isnardd, M. A. Gusmão and J. B. M. da Cunha, *J. Alloys Compd.*, 2010, **491**, 41–44.

39 J. Titiš and R. Bocă, *Inorg. Chem.*, 2011, **50**, 11838–11845.